Strongly nonlinear internal soliton load on a small vertical circular cylinder in two-layer fluids

Jieshuo Xie [a,b,c], Yongjun Jian [a,b,c,*], Liangui Yang [a]

[a] School of Mathematical Science, Inner Mongolia University, Hohhot 100080, PR China
[b] Ocean Engineering Research Center, School of Engineering, Zhongshan University, Guangzhou 510275, PR China
[c] Guangdong Province Key Laboratory of Coastal Ocean Engineering, Zhongshan University, Guangzhou 510275, PR China

ARTICLE INFO

ABSTRACT

The solutions of MCC theory are used to investigate larger-amplitude strongly nonlinear internal soliton load on a small surface-piercing circular cylinder in two-layer fluids. By comparing the wave profiles and instantaneous horizontal velocities calculated by MCC theory with those of KdV theory and experimental data, we verify the validity of MCC theory for larger-amplitude strongly nonlinear internal soliton. The accelerations are computed, and then force and torque on a small cylinder are estimated based on Morison's formula for both MCC and KdV theories. Computed results show that the internal soliton force and torque become more and more large and wide with the increase of amplitude for MCC theory. The location of torque crest calculated by MCC theory departs from origin (moving to the right) as the amplitude grows and whenever the inertial term is included or not, the wave forces computed based on the two theories both have small discrepancies for the same amplitude, but when the inertial term is included, the torque obtained by MCC theory will be much larger and the torque obtained by KdV still have a small discrepancy. The reasons are presented in detail. The internal wave force will be underestimated if the traditional KdV theory is used. Therefore, ocean engineers should consider the large-amplitude strongly nonlinear internal soliton load on marine construct carefully.

© 2009 Elsevier Inc. All rights reserved.

1. Introduction

Wave-structure interaction has received a significant attention in the literature under the assumption of the linear theory of water waves in the case of a single homogeneous fluid of constant density. Also some researches on nonlinear theory in a single homogeneous fluid have been given. As to two-dimensional case in a single homogeneous fluid, some of the classical investigations on wave interaction with rigid obstacles are given by [1–3]. In the three-dimensional situation, MacCamy and Fuchs [4] obtained a closed form solution to evaluate the dynamic pressures, forces and moments on a single large vertical circular cylinder subjected to linear plane waves being diffracted around a large vertical cylinder. The paper [5] carried out the study on the diffraction of three-dimensional short-crested waves on a circular cylinder and found that wave loads induced by short-crested waves on a circular cylinder are always less than those induced by plane waves with the same total wave number. Jian et al. [6,7] studied the short-crested wave-current forces around a large vertical circular cylinder including the effect of uniform currents and third order approximation to capillary gravity short crested waves with uniform currents, respectively. They found that with the increase of current speed, the water run-up on the cylinder, total wave loads,

* Corresponding author. Address: School of Mathematical Science, Inner Mongolia University, Hohhot 100080, PR China. Tel.: +86 471 4992946 8313; fax: +86 471 4991650.
E-mail address: jianyongjun@yahoo.com.cn (Y. Jian).

the crests of wave profile and wave pressure will exceeds that of long crested plane wave and short-crested wave case without currents even though the current speed is small.

All the aforementioned wave-structure interaction problems are analyzed in a single fluid domain of homogeneous density. However, waves can also exist at the interface of two immiscible liquids having two different densities. Such a sharp density gradient can, for example, be generated in the ocean by solar heating of the upper layer, or in an estuary or a fjord into which fresh less saline river water flows over oceanic water, which is more saline and consequently heavier [8]. Internal solitons are usually generated by a tidally driven flow over sills, continental shelf edges, or other major variations in underwater topography. Recent observations show that large-amplitude internal waves frequently occur, see for instance [9,10]. A collection of synthetic aperture radar (SAR) images in different ocean basins shows that large-amplitude internal waves are a common phenomenon in the oceans. In order to continue deep-sea drilling for oil in areas where these internal solitons occur, the drilling rigs will have to be built to withstand these forces (see for example [11]). The paper [12] conducted experimental investigations on internal solitary wave propagation and their reflection from a smooth uniform slope in a two-layered fluid system with a free surface. The soliton perturbation theory is used in [13] to study the solitons that are governed by the generalized KdV equation in the presence of perturbation terms.

Starting from the Euler system governing the motion of each fluid layer, the classical weakly nonlinear theories of long-wave motion assume that the typical amplitude of the waves is small compared with both layer thicknesses, and the horizontal length scale of the motion is large with respect to both layer thicknesses. Due to a balance between nonlinear and dispersive effects, they retain their shape and speed during their propagation (see for example [14]). The typical representative includes well-known shallow water KdV equation, eKdV equation which is the extended form of KdV equation by adding the cubic nonlinear term, deep water BO equation and intermediate long wave (ILW) equations. A useful extension of the weakly nonlinear two-layer eKdV model was proposed by Miyath, Choi and Camassa, Helfrich and Melville called the extension as MCC equation, which was derived from their name's acronyms (see for example [15–18]). They each derived equivalent two-layer models with full nonlinearity, and no smallness assumption on the wave amplitude is made.

In the present work, our research interest is focused on the large-amplitude internal soliton load on a small vertical circular cylinder. The paper [19] put forward an empirical formula to compute the forces associated with surface waves on piles. The Morison equation was formulated with the assumption that the presence of the object did not affect the characteristics of the wave field. Therefore, once velocity field is known, the force and torque can be obtained. Basing on Morison's empirical formula the papers [20–22] used weakly nonlinear KdV equation to estimate the horizontal velocity and its acceleration in a vertical section for computing the force and torque on a supposed pile in a continuous stratified fluid. However, no-one seems to have discussed, to the authors' knowledge, the load of strongly nonlinear large-amplitude internal soliton on a small vertical circular cylinder.

In this paper, the MCC equation and KdV equation were used to investigate wave profiles, horizontal velocity and acceleration distributions, respectively. Then the comparison of the above theoretical results was made with those of experiment in [23]. Results show that for strongly nonlinear large-amplitude internal soliton, the MCC theory is more effective than the KdV theory. Furthermore, we calculate the internal soliton force and torque for several typical amplitudes based on Morison's empirical formula. Detailed results are presented and discussed for the force and torque of a small cylinder produced by strongly nonlinear large-amplitude internal soliton.

2. MCC equation and KdV equation

Since our study is based on the MCC equation, it is necessary to introduce this theory briefly (refer to [17,18]). Moreover, we will illustrate the relationship between MCC theory and KdV theory.

Consider one-dimensional internal solitons propagating along the interface between two homogeneous incompressible and inviscid fluid of different density. Fig. 1 shows a two-layer fluid system that is stably stratified. The origin of the axes
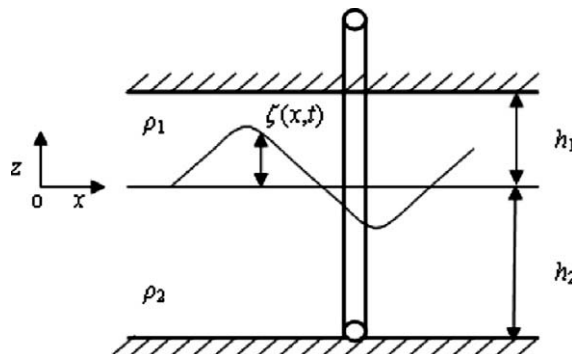

Fig. 1. Definition sketch of two-fluid system in appearance of a small vertical circular cylinder.

will be located in the undisturbed interface such that oz points vertically downwards. We assume that the upper and lower fluid have constant densities ρ_1 and ρ_2 ($>\rho_1$) with constant depths h_1 and h_2, respectively. Interfacial displacement is designated as $\zeta(x, t)$. A small vertical circular cylinder is located at $x = 0$ and extends from the rigid-lid approximated free surface to the horizontal bottom. We denote amplitude of the interfacial soliton as a, and its typical wavelength as L, then as we all known, $\alpha = a/h$, $\varepsilon = h_1/L$ are the two important parameters to describe nonlinearity and dispersion.

Based on the above assumption, the velocity components in Cartesian coordinates (u_i, w_i) and the pressure p_i satisfy the continuity equation and the Euler equations

$$u_{ix} + w_{iz} = 0, \tag{1}$$

$$u_{it} + u_i u_{ix} + w_i u_{iz} = -p_{ix}/\rho_i, \tag{2}$$

$$w_{it} + u_i w_{ix} + w_i w_{iz} = -p_{iz}/\rho_i - g, \tag{3}$$

where g is the gravitational acceleration and subscripts with respect to space and time represent partial differentiation. In a two-fluid system, $i = 1$ ($i = 2$) stands for the upper (lower) fluid (see Fig. 1).

The boundary conditions at the interface are the continuity of normal velocity and pressure:

$$\zeta_t + u_1 \zeta_x = w_1, \quad \zeta_t + u_2 \zeta_x = w_2, \quad p_1 = p_2 \quad \text{at } z = \zeta(x, t) \tag{4}$$

at the upper and lower rigid surfaces, the kinematics boundary conditions are given by

$$w_1(x, h_1, t) = 0, \quad w_2(x, -h_2, t) = 0. \tag{5}$$

From the assumption that the thickness of each fluid layer is much smaller than the typical wavelength, the continuity equation (1) yields the following scaling relation

$$\frac{w}{u} = O\left(\frac{h}{L}\right) = O(\varepsilon) \ll 1 \tag{6}$$

for finite-amplitude waves, there is the following important scaling relation

$$u_i/U_0 = O(\zeta/h_i) = O(\alpha) = O(1), \tag{7}$$

where $U_0 = (gh_1)^{1/2}$ is the typical velocity. Under the assumption of (7), solving Eqs. (1)–(5) by layer-mean integration and systematic asymptotic expansion method, we obtain the following strongly nonlinear internal wave equation, which is so-called MCC equation

$$\eta_{1t} + (\eta_1 \overline{u_1})_x = 0, \quad \eta_1 = h_1 - \zeta, \tag{8}$$

$$\eta_{2t} + (\eta_2 \overline{u_2})_x = 0, \quad \eta_2 = h_2 + \zeta, \tag{9}$$

$$\bar{u}_{1t} + \bar{u}_1 \bar{u}_{1x} + g\zeta_x = -\frac{P_x}{\rho_1} + \frac{1}{\eta_1}\left(\frac{1}{3}\eta_1^3 G_1\right)_x + O(\varepsilon^4), \tag{10}$$

$$\bar{u}_{2t} + \bar{u}_2 \bar{u}_{2x} + g\zeta_x = -\frac{P_x}{\rho_2} + \frac{1}{\eta_2}\left(\frac{1}{3}\eta_2^3 G_2\right)_x + O(\varepsilon^4), \tag{11}$$

where

$$\overline{u_1}(x, t) = \frac{1}{\eta_1}\int_{\zeta}^{h_1} u_1(x, z, t)\,dz, \quad \overline{u_2}(x, t) = \frac{1}{\eta_2}\int_{-h_2}^{\zeta} u_2(x, z, t)\,dz,$$

$$P(x, t) = p_2(x, \zeta, t), \quad G_i(x, t) = \overline{u_{ixt}} + \overline{u_i u_{ixx}} - (\overline{u_{ix}})^2.$$

The MCC equations are gained through the finite-amplitude wave assumption (7). If we assume the amplitude is small corresponding to (7), the following scaling relation

$$u_i/U_0 = O(\zeta/h_i) = O(\alpha) = O(\varepsilon^2) \tag{12}$$

is satisfied. Under this scaling relation, the nonlinear dispersive terms of $O(\varepsilon^2)$ in the right-hand sides of (10) and (11) reduce to

$$\frac{1}{\eta_i}\left(\frac{1}{3}\eta_i^3 G_i\right)_x \rightarrow \frac{1}{3}h_i^2 \overline{u_{ixxt}}.$$

Thus the MCC equation (8)–(11) reduce to the weekly nonlinear internal wave equations

$$\eta_{1t} + (\eta_1 \overline{u_1})_x = 0, \quad \eta_1 = h_1 - \zeta, \tag{13}$$

$$\eta_{2t} + (\eta_2 \overline{u_2})_x = 0, \quad \eta_2 = h_2 + \zeta, \tag{14}$$

$$\bar{u}_{1t} + \bar{u}_1 \bar{u}_{1x} + g\zeta_x = -\frac{P_x}{\rho_1} + \frac{1}{3}h_1^2 \overline{u_{1xxt}} + O(\varepsilon^4), \tag{15}$$

$$\bar{u}_{2t} + \bar{u}_2 \bar{u}_{2x} + g\zeta_x = -\frac{P_x}{\rho_2} + \frac{1}{3}h_2^2 \overline{u_{2xxt}} + O(\varepsilon^4), \tag{16}$$

to look for waves of permanent form traveling from left to right with constant speed c, we make the analysis

$$\zeta(x,t) = \zeta(X), \quad \bar{u}_i(x,t) = \bar{u}_i(X), \quad X = x - ct \tag{17}$$

simplify the MCC equation (8)–(11) using (17), the solution can be expressed by a nonlinear ordinary differential equation

$$(\zeta_X)^2 = \left[\frac{3g(\rho_2 - \rho_1)}{c^2(\rho_1 h_1^2 - \rho_2 h_2^2)}\right]\frac{\zeta^2(\zeta - a_-)(\zeta - a_+)}{(\zeta - a_*)}, \tag{18}$$

where $a_* = -h_1 h_2(\rho_1 h_1 + \rho_2 h_2)/(\rho_1 h_1^2 - \rho_2 h_2^2), a_-, a_+$ satisfy $a_- < a_+$ and are the two roots of the following quadratic equation

$$\zeta^2 + q_1\zeta + q_2 = 0, \tag{19}$$

where $q_1 = -c^2/g - h_1 + h_2$, $q_2 = h_1 h_2(c^2/c_0^2 - 1)$.

The expression (18) is an ordinary differential equation which does not explicitly contain X, after suitable transform and elliptic integrals, its solution in the form of $X = X(\zeta)$ can be derived. From (19), the amplitude of the highest traveling waves is

$$a_m = \frac{h_1 - h_2(\rho_1/\rho_2)^{1/2}}{1 + (\rho_1/\rho_2)^{1/2}}. \tag{20}$$

If the amplitude goes beyond the limit, it will cause the Helmholtz instability (see Ref. [23]), and the solution expressed by (18) does not exist.

Similarly, using (17), after simplifying the weakly nonlinear internal wave equations (13)–(16), we can get the KdV equation as follow

$$\zeta_t + c_0\zeta_x + c_1\zeta\zeta_x + c_2\zeta_{xxx} = 0, \tag{21}$$

where $c_0^2 = \frac{gh_1 h_2(\rho_2 - \rho_1)}{(\rho_1 h_2 + \rho_2 h_1)}, c_1 = -\frac{3c_0}{2}\frac{\rho_1 h_2^2 - \rho_2 h_1^2}{(\rho_1 h_1 h_2^2 + \rho_2 h_1^2 h_2)}, c_2 = \frac{c_0}{6}\frac{\rho_1 h_1^2 h_2 + \rho_2 h_1 h_2^2}{(\rho_1 h_2 + \rho_2 h_1)}$.

The solitary wave solution is given by

$$\zeta_{KdV}(X) = a\sec h^2(X/\lambda_{KdV}), \quad X = x - ct, \tag{22}$$

where $(\lambda_{KdV})^2 = 12c_2/(ac_1)$, $c = c_0 + a c_1/3$.

Now we have described the strongly nonlinear internal wave equation (8)–(11) and the weakly nonlinear internal wave equation (13)–(16), and the solutions (18) and (22) correspond to them as well.

3. Internal soliton profile, instantaneous velocity and acceleration

As to large-amplitude internal waves, the paper [23] got wave profiles and instantaneous velocities by direct numerical simulation for original Euler equations, and then compared with KdV theory and experimental data, respectively. Result showed the method of direct numerical simulation for the strongly nonlinear large-amplitude internal wave is more reasonable than that of KdV theory. In Ref. [24], Camassa et al. used the strongly nonlinear internal wave MCC equation to calculate the wave profiles and instantaneous velocities, and compared with the experimental data collected by Grue et al. [23]. Computational result has a good agreement with those of experiment for large-amplitude internal soliton, but the comparison of the result of KdV theory with that of MCC theory and experiment has not been given in Ref. [24]. As we want to show the MCC theory is much more reasonable than KdV theory, we think the comparison is needed to be given although there are many similarities with the comparison of Grue and Camassa has done.

In this section, we compare the experimental data given by Grue [23] with those of MCC and KdV theoretical results. Moreover, in order to calculate the load, the result of acceleration is computed.

In order to compare theoretical results with those of Grue's experiment, we choose parameters $h_2/h_1 = 4.13$, $\rho_1 = 999$ kg/m^3, $\rho_2 = 1022$ kg/m^3, which are the same as Grue's experiment (If no special statement, the selection of these parameters is the same as the above in the following computation.) By (20) we can calculate the maximum wave amplitude $a_m = 1.55$. So the actually existed amplitude will less than a_m. In the Sections 3.1 and 3.2, we calculate wave profiles and velocities in the case of several typical amplitudes and compare them with those of experimental data. In Section 3.3, we first give the variation of maximum acceleration with amplitude, and then acceleration corresponding to the same several typical amplitudes with which used to calculate wave profiles and velocities.

3.1. Wave profiles

Fig. 2 illustrates the MCC wave profiles calculated from (18) using forth-order Rouger–Kutta method for several typical amplitudes. This figure is almost the same with that gained by Grue et al. [23], but the calculated method is different. What we must say is that Fig. 2 is almost the same with what Camassa [24] has done except that the result of KdV theory has been added in order that we can have a comparison. Initial condition at the location $X = 0$ was prescribed corresponding to the above typical amplitudes. The KdV wave profiles can be obtained directly from (22). We can see from Fig. 2a and b that when amplitude is small, both the MCC and KdV theoretical results have a good agreement with experimental data. However, with
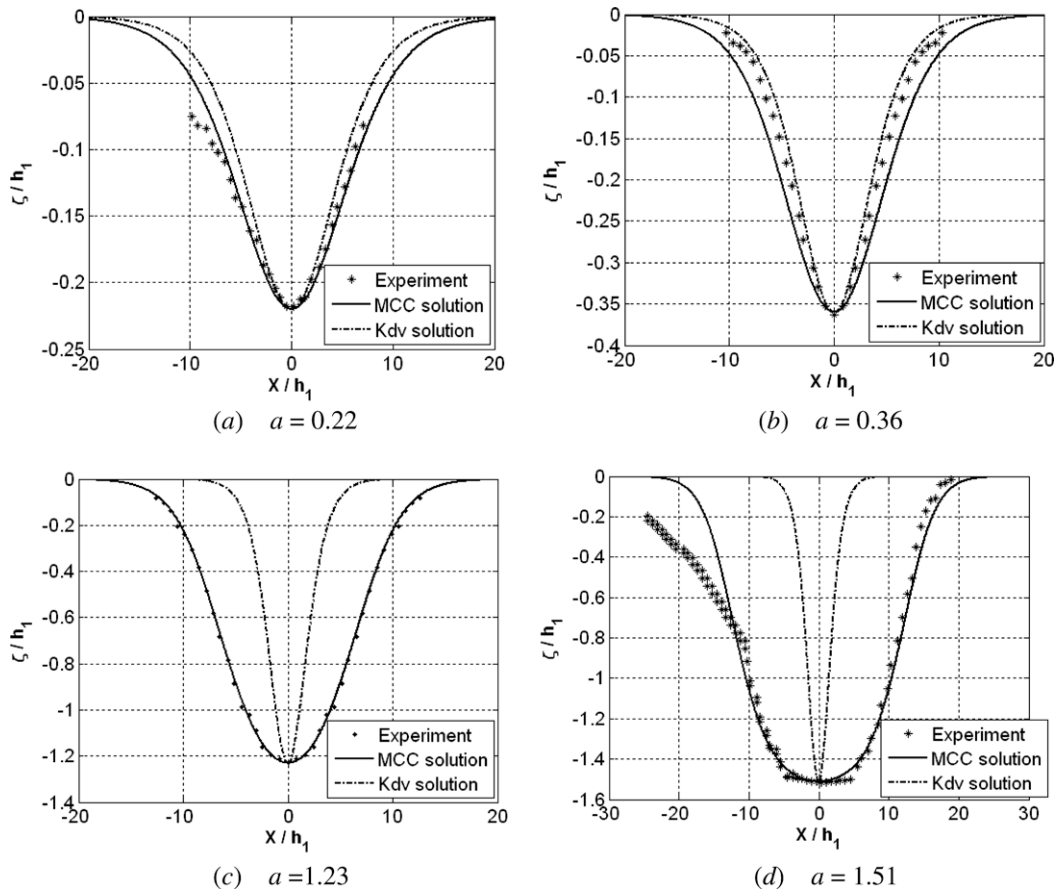
Fig. 2. Wave profiles of MCC theory, KdV theory and experimental data for different amplitudes.

the increase of the amplitude (see Fig. 2c and d), the weakly nonlinear KdV theory become invalid, and only the MCC results have a good agreement with experimental data. After more careful analysis, we find that when $a < 0.4$, the KdV theory still work well, but as the amplitude is larger than 0.4, the discrepancy begin to happen apparently. Moreover, the property of being wider and wider of wave profiles can be found from Fig. 2c and d in the case of large-amplitude.

3.2. Instantaneous horizontal velocity

An approximate relation between layer-averaged velocities and instantaneous horizontal velocity obtained by particle imaging velocimetry (PIV) measurement (In Ref. [24]) for the shallow-water configuration is

$$u_2(x,z,t) = \overline{u_2}(x,t) + \left(\frac{(\eta_2(x,t))^2}{6} - \frac{(z+h_2)^2}{2} \right) \partial_x^2 \overline{u_2}(x,t). \tag{23}$$

Substituting (17) into (8) and (9) and integrating once with respect to X gives

$$\overline{u_2}(X) = c\left(1 - \frac{h_2}{\eta_2(X)} \right). \tag{24}$$

Putting (24) into (23), we get the instantaneous horizontal velocity of lower fluid

$$u_2(X,z) = c\left[1 - \frac{h_2}{\eta_2} + \left(\frac{\eta_2^2}{6} - \frac{(z+h_2)^2}{2} \right) \left(\frac{h_2\eta_2''}{\eta_2^2} - \frac{2h_2(\eta_2')^2}{\eta_2^3} \right) \right]. \tag{25}$$

Similarly, the instantaneous horizontal velocity for upper fluid can be written as

$$u_1(X,z) = c\left[1 - \frac{h_1}{\eta_1} + \left(\frac{\eta_1^2}{6} - \frac{(h_1-z)^2}{2} \right) \left(\frac{h_1\eta_1''}{\eta_1^2} - \frac{2h_1(\eta_1')^2}{\eta_1^3} \right) \right]. \tag{26}$$
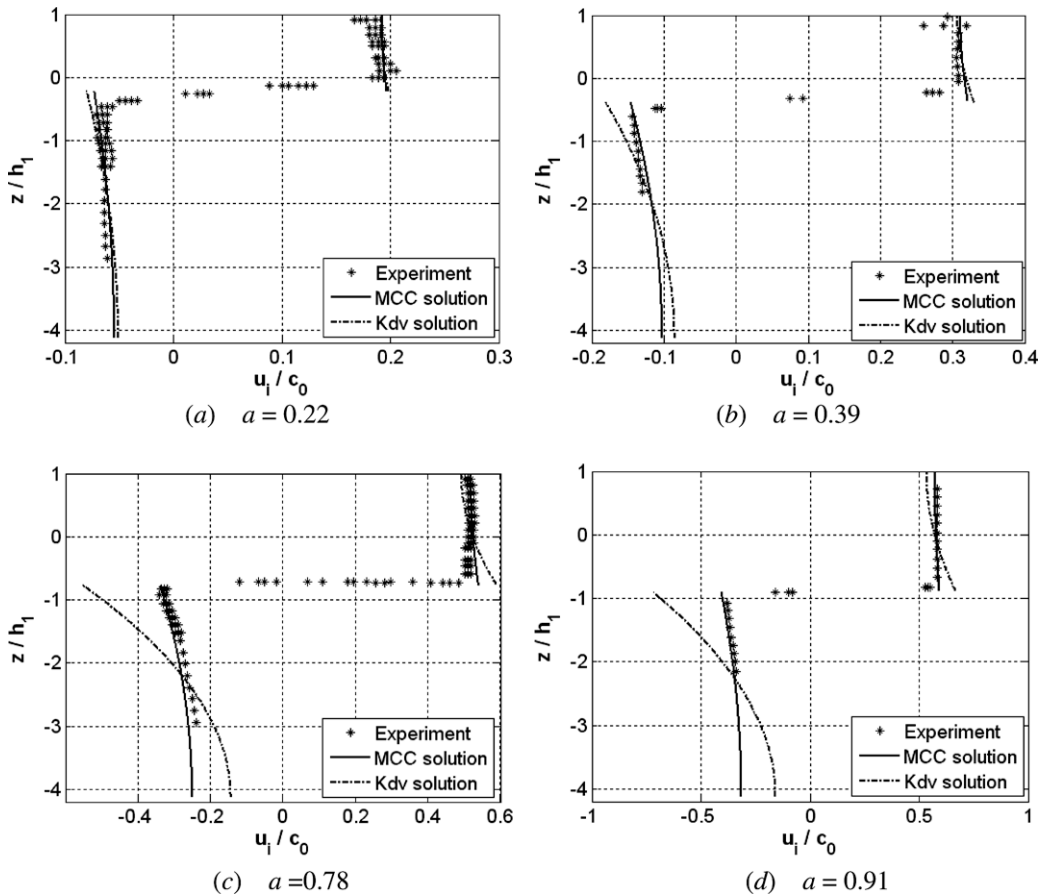
Fig. 3. Instantaneous horizontal velocities of MCC theory, KdV theory and experimental data for different amplitudes.

After substituting the interfacial displacements (18) and (22) for MCC and KdV theory respectively into (25) and (26), the value of instantaneous horizontal velocity can be gained. Fig. 3 gives the instantaneous horizontal velocity at wave-crest for several different amplitudes. This figure is also almost the same with that gained by Grue et al. [23], but the calculated method used here is different too. Similar to the analysis of wave profiles in Fig. 2, we still can see that for small amplitude internal soliton, both MCC and KdV theories is valid (see Fig. 3a and b). However, for larger-amplitude internal soliton, only the MCC theory behaves a good agreement with experimental data (see Fig. 3c and d).

3.3. Horizontal acceleration

From (25) and (26), horizontal acceleration of both upper and lower layer fluids can be calculated by differentiating the velocity concerning the time. The results can be expressed as

$$
\frac{\partial u_1}{\partial t} = -c\frac{\partial u_1}{\partial X}
$$
$$
= c\left[-\frac{h_1\zeta_X}{\eta_1^2} - \frac{\eta_1\zeta_X}{3}\left(\frac{h_1\eta_1''}{\eta_1^2} - \frac{2h_1(\eta_1')^2}{\eta_1^3}\right) + h_1\left(\frac{\eta_1^2}{6} - \frac{(h_1-z)^2}{2}\right)\left(\frac{\eta_1'''\eta_1 + 2\eta_1''\zeta_X}{\eta_1^3} - \frac{4\eta_1\eta_1'\eta_1'' + 6(\eta_1')^2\zeta_X}{\eta_1^4}\right)\right], \tag{27}
$$

$$
\frac{\partial u_2}{\partial t} = -c\frac{\partial u_2}{\partial X}
$$
$$
= c\left[\frac{h_2\zeta_X}{\eta_2^2} + \frac{\eta_2\zeta_X}{3}\left(\frac{h_2\eta_2''}{\eta_2^2} - \frac{2h_2(\eta_2')^2}{\eta_2^3}\right) + h_2\left(\frac{\eta_2^2}{6} - \frac{(z+h_2)^2}{2}\right)\left(\frac{\eta_2'''\eta_2 - 2\eta_2''\zeta_X}{\eta_2^3} - \frac{4\eta_2\eta_2'\eta_2'' - 6(\eta_2')^2\zeta_X}{\eta_2^4}\right)\right], \tag{28}
$$

substituting wave profiles of MCC and KdV theory (18) and (22) into (27) and (28), we can get the acceleration for upper and lower layer fluids, respectively.
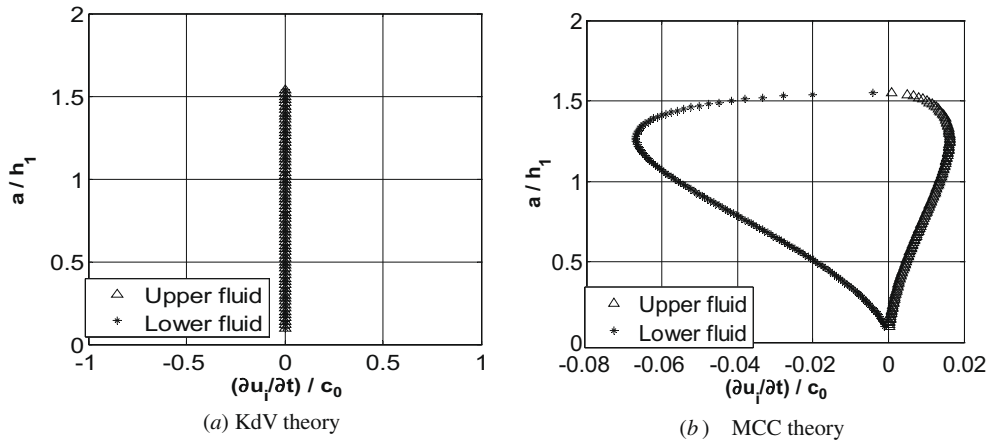
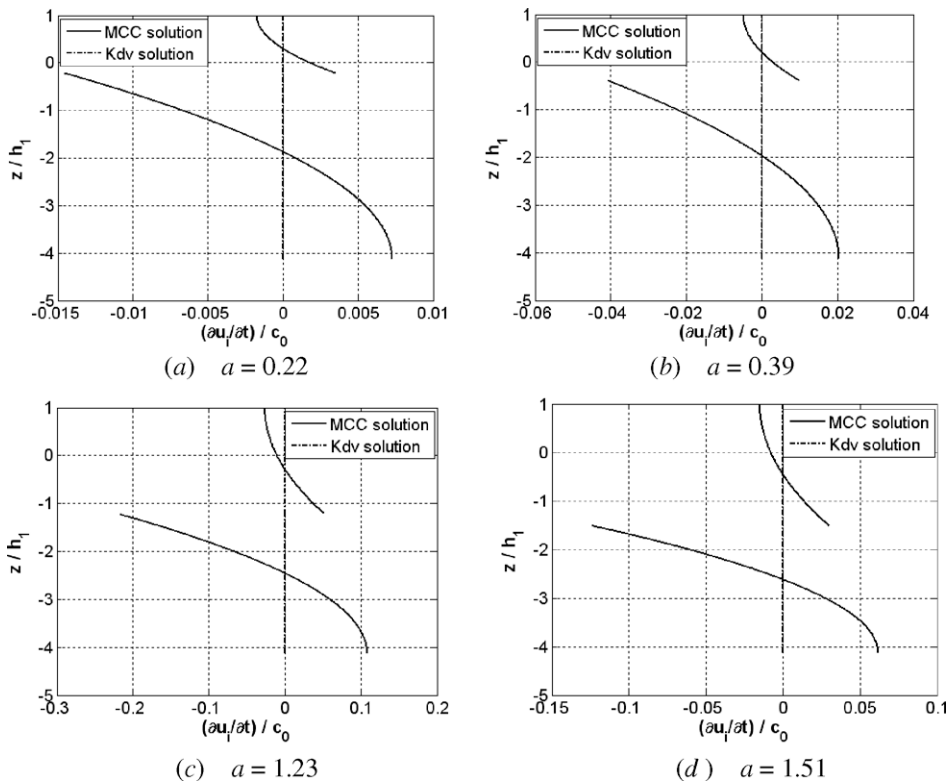**Fig. 4.** The variations of maximum acceleration with different amplitudes.

Fig. 5. The acceleration at wave-crest for several different amplitudes.

Fig. 4 illustrates the variations of maximum acceleration with amplitudes. From Fig. 4, we can see an apparently difference, that is, the maximum acceleration of KdV is always the trivial value, zero, but the maximum acceleration of MCC theory changes continuously concerning amplitude, which is not zero, for both upper and lower layer fluids. This difference is agreement with the assumption of the two theories, as the assumption (12) of KdV theory is that the relative scale of interfacial amplitude is the order of $O(\varepsilon^2)$ which leads to the local acceleration at the order of $O(\varepsilon^2)$ then it can be canceled, while the assumption (7) of MCC theory is that the relative scale of interfacial amplitude has the order of $O(1)$ which leads to the local acceleration at the order of $O(\varepsilon^2)$ then it should be preserved. So we think the numerical result of maximum acceleration in Fig. 4b calculated by (27) and (28) is reasonable.

Fig. 5 shows the acceleration at wave-crest for several different amplitudes. Seen from Fig. 5, an important property of acceleration can be found, that is, both the acceleration in upper and in lower layer fluid are approximately negatively

symmetric about the center (where the acceleration of KdV theory is zero). Thus the directions of the accelerations at the two sides of the center are opposite and the magnitudes are equal approximately. This property is very important in calculating the load of internal soliton on the small cylinder. In Section 4, we will give how this property has an influence to load.

4. Horizontal forces and torque

As we have known, when calculating the wave force on a small cylindrical structure, the empirical Morison's formula is always used. In this formula, the force F includes two parts: one is called drag force, which is noted as F_D, the other is called inertial force, which is noted as F_I. In this section, we use MCC and KdV theories to compute the load on a small cylinder with and without the inertial force.

From the Section 3.3, we can see that the inertial term is always small when the load of nonlinear internal wave is estimated using the KdV theory. However, due to the scale of acceleration for MCC theory being the order of $O(1)$, so the inertial force need to be analyzed carefully.

4.1. Horizontal forces

For the upper fluid, inertial and drag forces are

$$F_{I1} = \int_\zeta^{h_1} C_m \rho_1 \pi \frac{D^2}{4} \frac{\partial u_1(X,z)}{\partial t} \, dz, \quad F_{D1} = \int_\zeta^{h_1} C_d \rho_1 \frac{D}{2} u_1(X,z)|u_1(X,z)| \, dz,$$

similarly, for the lower fluid, inertial and drag forces can be written as

$$F_{I2} = \int_{-h_2}^\zeta C_m \rho_2 \pi \frac{D^2}{4} \frac{\partial u_2(X,z)}{\partial t} \, dz, \quad F_{D2} = \int_{-h_2}^\zeta C_d \rho_2 \frac{D}{2} u_2(X,z)|u_2(X,z)| \, dz.$$

It is worth being noticed that as our main attention is focused on large-amplitude internal waves, the displacement of interface can not be neglect. Different from those of KdV theory, where the integral limit of upper or lower is zero, the integral limit of upper or lower in the above expression of the force is ζ.

In the following computation, we choose $C_m = 2.0$, $C_d = 1.2$, $D = 5$ m, $h_1 = 50$ m, which we want them to consist with most of the practical computation. From Sections 3.1 and 3.2, it can be concluded that MCC theory may be more reasonable than KdV theory in calculating the large-amplitude internal soliton. Thus we use MCC theory to estimate the force and torque for different amplitudes, and compare the result with KdV theory.

Ignoring the inertial term, we express the total forces in upper and lower fluids as

$$F_1 = \int_\zeta^{h_1} C_d \rho_1 \frac{D}{2} u_1(X,z)|u_1(X,z)| \, dz, \tag{29}$$

$$F_2 = \int_{-h_2}^\zeta C_d \rho_2 \frac{D}{2} u_2(X,z)|u_2(X,z)| \, dz \tag{30}$$

if the inertial term is included, the total force can be written as

$$F_1 = \rho_1 \int_\zeta^{h_1} \left(C_d \frac{D}{2} u_1(X,z)|u_1(X,z)| + C_m \pi \frac{D^2}{4} \frac{\partial u_1(X,z)}{\partial t} \right) dz, \tag{31}$$

$$F_2 = \rho_2 \int_{-h_2}^\zeta \left(C_d \frac{D}{2} u_2(X,z)|u_2(X,z)| + C_m \pi \frac{D^2}{4} \frac{\partial u_2(X,z)}{\partial t} \right) dz. \tag{32}$$

Fig. 6 shows the variations of internal wave forces with X computed by (29)–(32) on a small cylinder for several different amplitudes. Both MCC and KdV theories are used. It can be found from Fig. 6c and d that with the increase of the amplitude, the wave forces obtained from MCC theory become larger and wider than those of KdV theory. These results consist with the nature of the wave profiles in Fig. 2. Furthermore, we can see that the wave forces computed based on the two theories have small discrepancies for the same amplitude whenever the inertial term is included or not. The main reason is that the accelerations have the property that the directions are opposite and the magnitudes are approximately equal at the two sides of the center (see Fig. 5), so the inertial forces which are obtained from having an integral with acceleration term can be counteracted approximately.

4.2. Torque

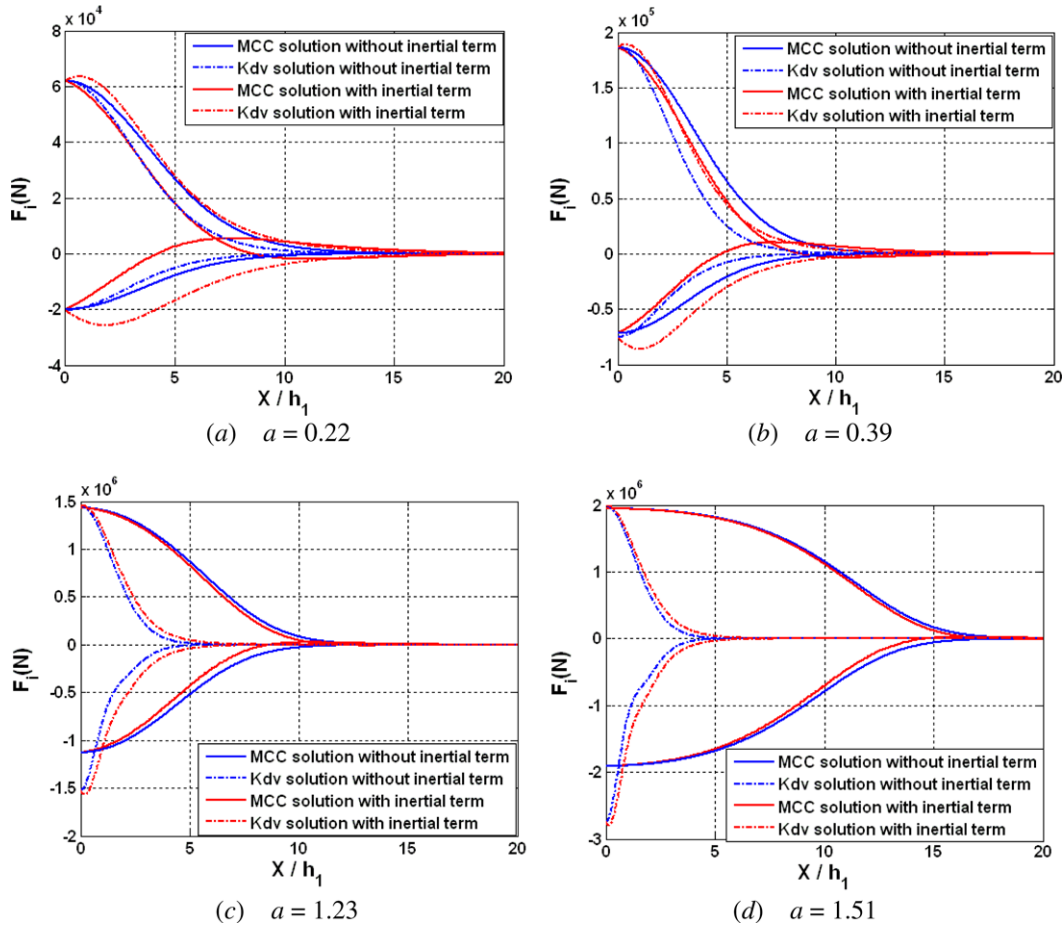Similar to the wave forces, we study the torque based on MCC and KdV theories with and without inertial term.

Fig. 6. The variations of internal wave forces with X for several different amplitudes with and without inertial term.

4.2.1. Torque without inertial term

If the inertial term is ignored, we call the total torque as drag force torque. When the fulcrum is located at the intersectant point between the cylinder and the interface, the drag force torque is

$$M_D = \int_\zeta^{h_1} (z - \zeta) C_d \rho_1 \frac{D}{2} u_1(X,z)|u_1(X,z)|\, dz + \int_{-h_2}^\zeta (z - \zeta) C_d \rho_2 \frac{D}{2} u_2(X,z)|u_2(X,z)|\, dz. \tag{33}$$

Fig. 7 showed the internal wave torque on a small cylinder calculated by (33) based on MCC and KdV theories for several different amplitudes. We can see from Fig. 7 that the torque obtained by MCC theory is larger than that of the KdV theory. Similar to the force, the torque calculated from MCC theory also gets broader and broader as the amplitude grows.

After analyzing the drag force torque by MCC theory and the maximum drag force torque got from the KdV theory in detail, we find an interesting phenomenon. Denote the horizontal location for soltion crest as O, from Fig. 7 we can get the maximum drag force torque at O for both MCC and KdV theories. These can be expressed as

$$\max M_{\text{DKdV}}(X) = M_{\text{DKdV}}(O), \tag{34}$$

$$\max M_{\text{DMCC}}(X) = M_{\text{DMCC}}(O), \tag{35}$$

we define the following ratio

$$\frac{M_{\text{DMCC}}(X) - \max M_{\text{DKdV}}(X)}{\max M_{\text{DKdV}}(X)} = R(X,a), \tag{36}$$

which is a function of X and amplitude a. This ratio means the relative difference between the drag force torque by MCC theory and the maximum drag force torque got from the KdV theory.

Fig. 8 gives the variations of the ratio $R(X,a)$ with X from (36) for different amplitudes 0.22, 0.40, 0.91, 1.23, 1.51 and1.55. The selection of other parameters in Fig. 8 is the same as the above. From Fig. 8, we can see that when X is fixed, then
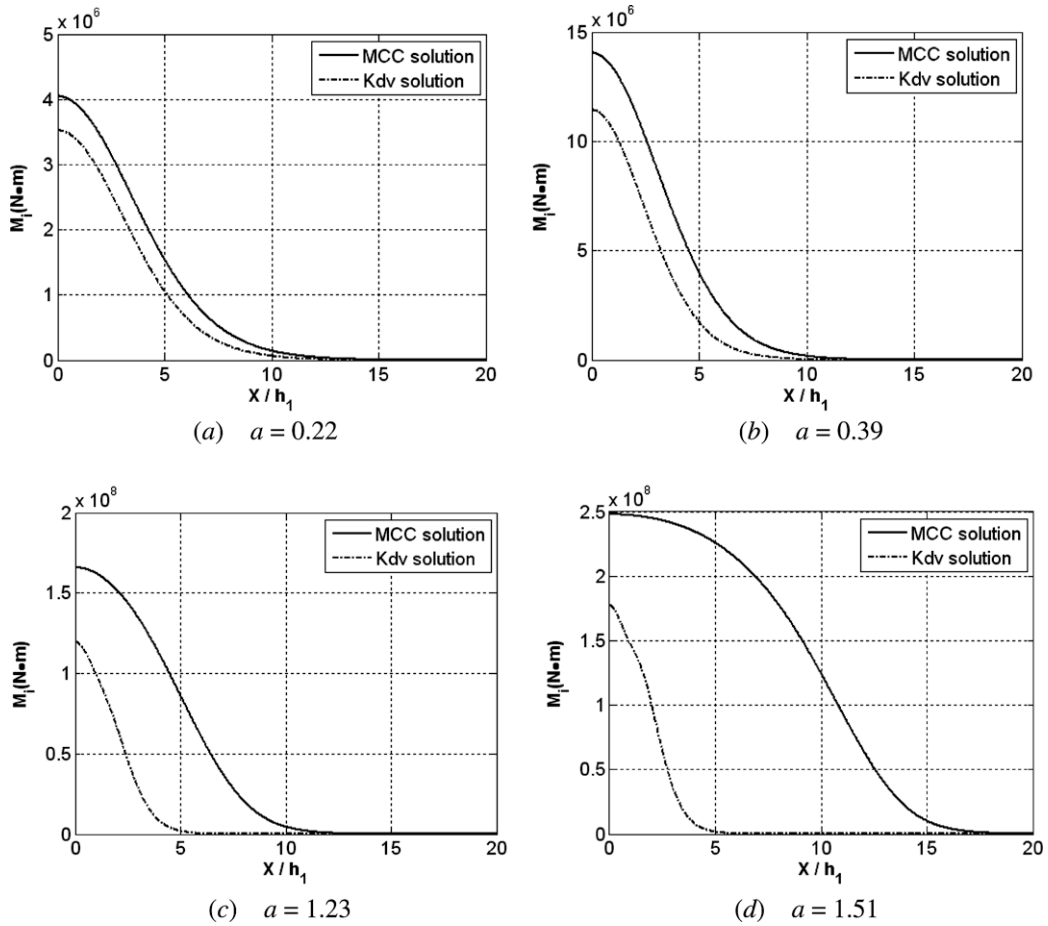
Fig. 7. The variations of internal wave torque with X for several different amplitudes without inertial term.
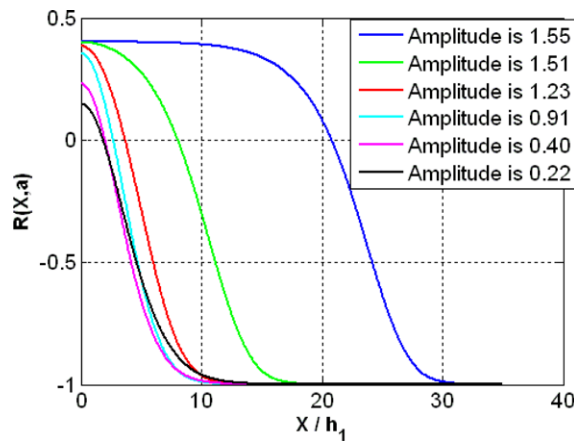

Fig. 8. The variations of the ratio $R(X,a)$ with X for different amplitudes.

$$R(X, a) < R(X, a_m),\tag{37}$$

where a_m equal to 1.55. By (36) and (37) we can get the relation between actual torque $M(X)$ and max M_{DKdV}

$$M(X) < \max M_{DKdV}(1 + R(X, a_m)).\tag{38}$$

Seeing from (38), we can conclude that when the maximum KdV solution max M_{DKdV} is solved, the upper limit of the actual torque can be obtained. For example, in the situation of Fig. 8, we can get the ratio $R(X, a_m)$ is 0.402, then

$$M(X) < 1.402 \max M_{DKdV}. \tag{39}$$

4.2.2. Torque with the inertial term

When the inertial term is included, the torque has the following formation

$$M_D = \rho_1 \int_{\zeta}^{h_1} (z - \zeta) \left[C_d \frac{D}{2} u_1(X, z) |u_1(X, z)| + C_m \pi \frac{D^2}{4} \frac{\partial u_1(X, z)}{\partial t} \right] dz$$

$$+ \rho_2 \int_{-h_2}^{\zeta} (z - \zeta) \left[C_d \frac{D}{2} u_2(X, z) |u_2(X, z)| + C_m \pi \frac{D^2}{4} \frac{\partial u_2(X, z)}{\partial t} \right] dz. \tag{40}$$

Fig. 9 gives the internal wave torque computed by (40) on a small cylinder for different amplitudes based on MCC and KdV theories. From Fig. 9, we find the torque obtained by MCC theory is much larger about 1000 times than those by KdV theory, and we think this is led by the assumption's difference of the two theories. Moreover, the location of torque crest calculated
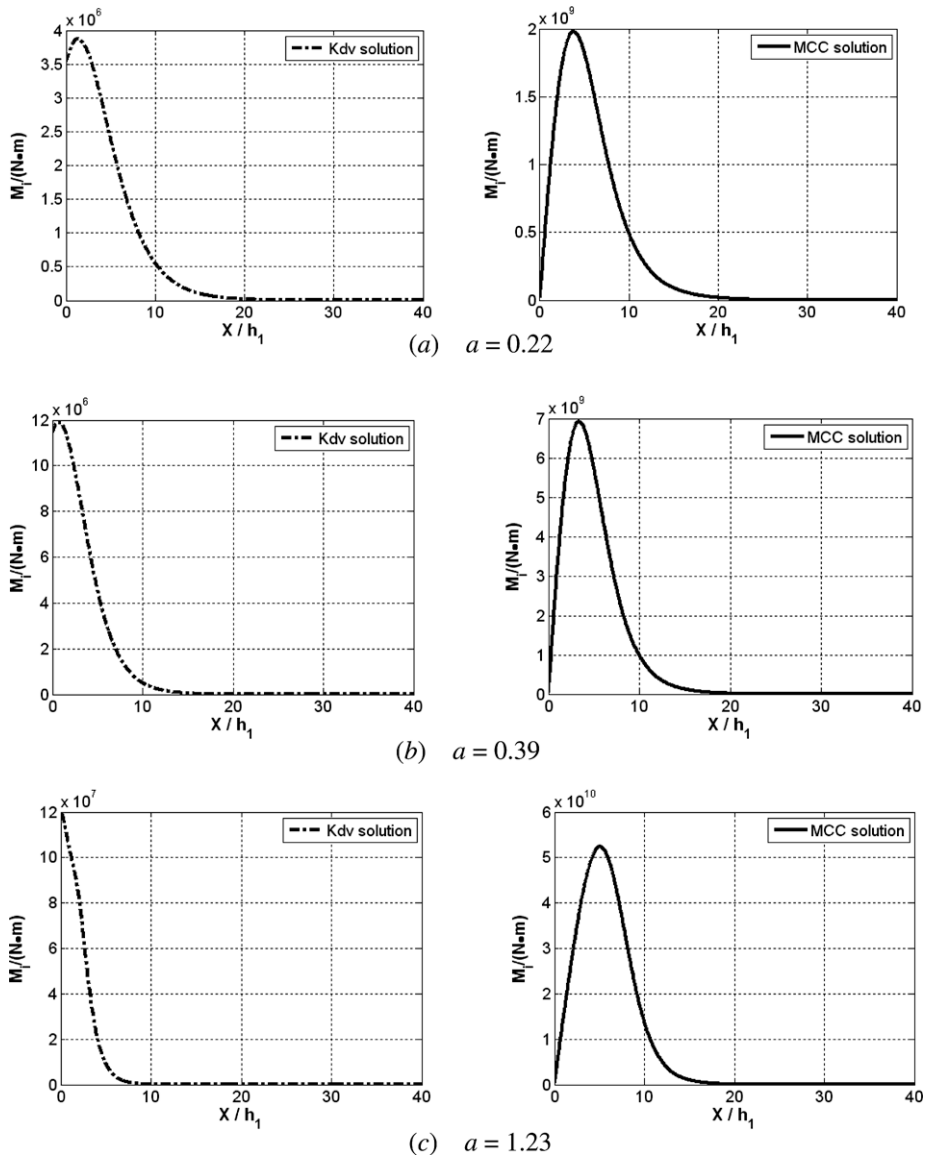

Fig. 9. The variations of internal wave torque with X for several different amplitudes with inertial term.
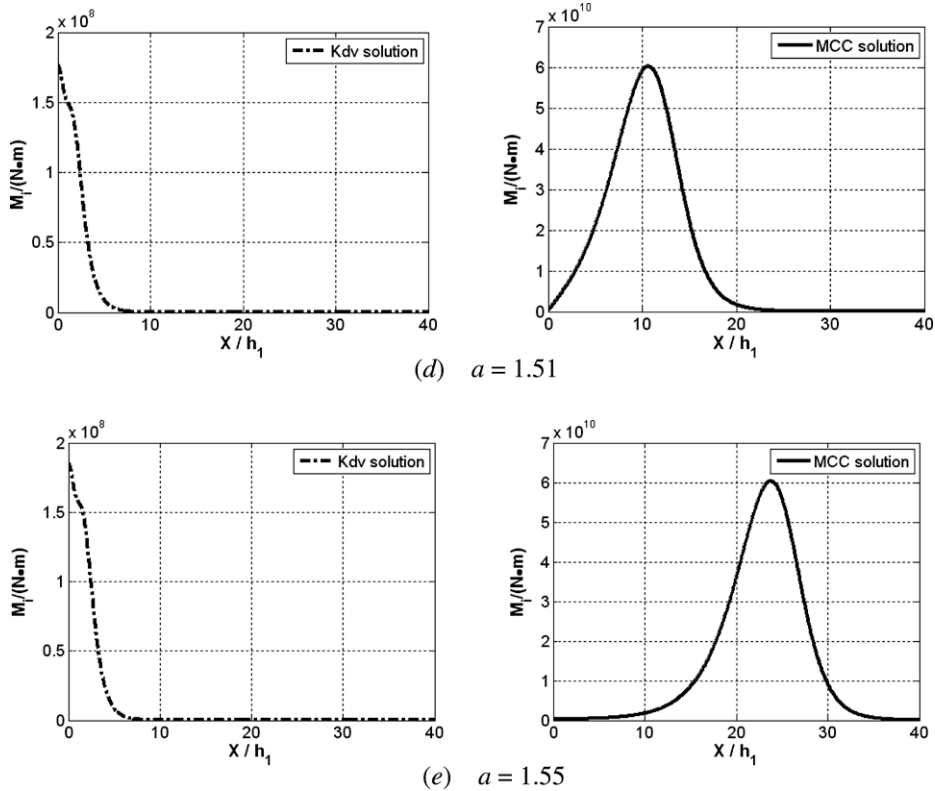
(d) $a = 1.51$

(e) $a = 1.55$

Fig. 9 (*continued*)

by MCC theory departs from origin (moving to the right) as the amplitude grows. The reason is mainly due to the widening of the large-amplitude internal wave profiles with the increase of the amplitude. The calculation of torque needs to consider the product of the force and positional vector. Thus the widening of wave profiles will change the location of the largest torque. The location of the largest torque should be where the product of force and positional vector is largest.

By comparing the numerical results in Fig. 9 based on MCC and KdV theories with those in Fig. 7 for the same amplitude, we find that when the inertial term is included, the torque behaves small change by KdV theory, while the torque changes greatly by MCC theory. The reason is that for MCC theory, due to the $O(1)$ order acceleration, the inertial force is the order of $O(1)$, so the torque can become very large due to the larger positional vector although the directions of the accelerations at the two sides of the center are opposite. While for KdV theory, the inertial force is the order of $O(\varepsilon^2)$, so the torque change little even for large positional vector.

5. Conclusions

The internal soliton force and torque on a single surface-piercing circular cylinder in a two-layer fluid are investigated. Results obtained by comparing the wave profiles and instantaneous horizontal velocities calculated by MCC theory and KdV theory with those of experimental data show that the MCC theory is very valid for large-amplitude strongly nonlinear internal soliton. Then based on Morison's formula, we calculate the force and torque for both MCC and KdV theories. The main conclusions about load can be made as follows:

(1) With the increase of the amplitude, the wave forces and torque obtained from MCC theory become larger and wider than those of KdV theory.
(2) The location of torque crest calculated by MCC theory departs from origin (moving to the right) as the amplitude grows.
(3) Whenever the inertial term is included or not, the wave forces computed based on the two theories both have small discrepancies for the same amplitude, but when the inertial term is included, the torque obtained by MCC theory will be much larger and the torque obtained by KdV still have a small discrepancy.

Therefore, ocean engineers should consider the large-amplitude strongly nonlinear internal soliton load on marine construct carefully. Further, results of the strongly nonlinear internal soliton load on a large vertical circular cylinder will be published in another paper.

Acknowledgments

References

[1] J.N. Newman, Propagation of water waves past long two-dimensional obstacles, J. Fluid Mech. 23 (1965) 23–29.
[2] J.W. Miles, Surface-wave scattering matrix for self, J. Fluid Mech. 28 (1967) 755–767.
[3] P. McIver, Wave forces on adjacent floating bridges, Appl. Ocean Res. 8 (2) (1986).
[4] R.C. MacCamy, R.A. Fuchs, Wave forces on piles: a diffraction theory, US Army Corps of Engineering, Beach Erosion Board, Technical Memorandum, vol. 69, 1954.
[5] S.P. Zhu, Diffraction of short-crested waves around a circular cylinder, Ocean Eng. 20 (4) (1993) 389–407.
[6] Y.J. Jian, J.M. Zhan, Q.Y. Zhu, Short crested wave-current forces around a large vertical circular cylinder, Eur. J. Mech. B-Fluids 27 (2008) 346–360.
[7] Y.J. Jian, Q.Y. Zhu, J. Zhang, Y.F. Wang, Third order approximation to capillary gravity short crested waves with uniform currents, Appl. Math. Model. 33 (2009) 2035–2053.
[8] P.S. Kumar, T. Sahoo, Scattering of surface and internal waves by rectangular dikes, J. Offshore Mech. Arctic Eng. 129 (2007) 306–317.
[9] T.P. Stanton, L.A. Ostrovsky, Observations of highly nonlinear solitons over the continental shelf, Geo. Res. Lett. 25 (1998) 2695–2698.
[10] T.F. Duda, J.F. Lynch, J.D. Irish, et al, Internal tide and nonlinear wave behavior in the continental slope in the northern South China Sea, IEEE J. Oceanic Eng. 29 (2004) 1105–1131.
[11] C.Y. Chen, J.R. Hsu, M.H. Cheng, H.H. Chen, C.F. Kuo, An investigation on internal solitary waves in a two layer fluid: propagation and reflection from steep slopes, Ocean Eng. 34 (1) (2007) 171–184.
[12] M. Antonova, A. Biswas, Adiabatic parameter dynamics of perturbed solitary waves, Commun. Nonlinear Sci. Numer. Simulat. 14 (3) (2009) 734–748.
[13] M.J. Ablowitz, P.A. Clarkson, Solitons, Nonlinear Evolution Equations and Inverse Scattering, Cambridge University, Cambridge, 1991.
[14] A.K. Liu, Analysis of nonlinear internal waves in the New York Bight, J. Geo. Res. 93 (C10) (1988) 12317–12329.
[15] M. Miyata, An internal solitary wave of large amplitude, La Mer. 23 (1985) 43–48.
[16] M. Miyata, Long internal waves of large amplitude: in nonlinear water waves, Tokyo: IUTAM Sympos. (1987) 399–406.
[17] W. Choi, R. Camassa, Fully nonlinear internal waves in a two-fluid system, J. Fluid Mech. 396 (1999) 1–36.
[18] K.R. Helfrich, W.K. Melville, Long nonlinear internal waves, Ann. Rev. Fluid Mech. 38 (2006) 395–425.
[19] J.R. Morison, M.P. O'Brien, J.W. Johnson, S.A. Schaff, Forces exerted by surface waves on piles petroleum transaction, Am. Inst. Mining Eng. (1950) 189–196.
[20] S.Q. Cai, S.G. Wang, X.M. Long, A method to estimate the forces exerted by internal solitons on cylindrical piles, Ocean Eng. 30 (2003) 673–689.
[21] S.Q. Cai, S.G. Wang, X.M. Long, A simple estimation of the force exerted by internal solitons on cylindrical piles, Ocean Eng. 33 (2006) 974–980.
[22] S.Q. Cai, X.M. Long, Wang SG, Forces and torques exerted by internal solitons in shear flows on cylindrical piles, Appl. Ocean Res. 30 (2008) 72–77.
[23] J. Grue, A. Jensen, P.O. Rusas, J.K. Sveen, Properties of large-amplitude internal waves, J. Fluid Mech. 380 (1999) 257–278.
[24] R. Camassa, W. Choi, H. Michallet, P.O. Rusas, J.K. Sveen, On the realm of validity of strongly nonlinear asymptotic approximations for internal waves, J. Fluid Mech. 549 (2006) 1–23.